

Bond ordering in flux phases

Yifan Liu* and Vivek Aji†

Department of Physics and Astronomy, University of California, Riverside, California 92521, USA

Contrary to canonical expectations we show that lattice translational symmetry breaking often accompanies uniformly ordered flux phases. We demonstrate this phenomena by studying a spinless-fermion model on a square lattice with nearest-neighbor repulsion. We find an array of flux patterns, as a function interaction strength and filling factor, that break time-reversal symmetry but may or may not preserve translational symmetry. A key finding is that the pattern of flux ordering does not uniquely determine the electronic properties. As such a class of new phases of matter are introduced that expand the candidate ground states in many body interacting systems.

I. INTRODUCTION

Periodic arrangement of magnetic fluxes engender new phases and phenomena in solid state systems. The most celebrated example is the Quantum Anomalous Hall (QAH) effect realized in the Haldane model [1]. A generalization of the model leads to the realization of the Quantum Spin Hall Effect (QSH)[2]. An analogous picture also explains the origin of the Quantum Hall effect in a two dimensional lattice made of coupled one dimensional chains and anomalous Hall effect in Fermi liquids [3–5]. These models describe systems without any inter-particle interactions but other single particle effects, such as Spin Orbit Interactions (SOC), lead to QAH and QSH.

Flux phases also appear as possible ground states of interacting many body systems. The staggered flux phase [6–8], d-density wave (DDW)[9] and "Flux" state in the double-exchange [10] model are examples where time reversal is broken and the unit cell is doubled. Translationally invariant flux phases, sometimes referred to as the Loop Current phase (LC), were proposed for a three band model with nearest neighbor interaction [11–13] and observed in underdoped cuprates[14–17]. Onsite Coulomb interaction in a tight binding model $\text{LaNiO}_3 / \text{LaAlO}_3$ hetero-structures [18, 19] and nearest neighbor repulsion on a Honeycomb lattice also lead to flux phases displaying the QAH effect [20]. However the latter results have been challenged by recent density matrix renormalization studies that find a charge density wave state at half filling[21] and a Lanczos algorithm study that finds no evidence of a topological state[22]. Recently ordered chiral orbital currents have been proposed as an explanation for the colossal magnetoresistance (CMR) in Ferrimagnetic $\text{Mn}_3\text{Si}_2\text{Te}_6$ [23].

The above considerations motivate a study of flux phases in general both for possible novel ground states and the nature of quantum phase transitions in such systems. In this letter we draw attention to an important aspect of interaction driven flux phases which has not been appreciated thus far. *The spatial pattern of fluxes do not uniquely specify the electronic sector of the low energy states.* In particular lattice translational symmetry breaking is intertwined with spatially uniform intra-unit cell flux ordering. Previous studies of flux phases have not considered such states and

the goal of this letter is to show that these class of states are energetically favorable among flux phases condensed by nearest neighbor repulsion. Interestingly translation breaking accompanying an LC pattern has been invoked to explain the time reversal breaking in kagome superconductors [24].

To illustrate the origin of the intertwined order consider spinless fermions on two sites:

$$H = t(c_1^\dagger c_2 + c_2^\dagger c_1) + V n_1 n_2 \quad (1)$$

Mean field studies that focus on flux phases recast interaction as

$$V c_1^\dagger c_1 c_2^\dagger c_2 = -V \phi_{12} i (c_1^\dagger c_2 - c_2^\dagger c_1) + V (n_1 + n_2) \quad (2)$$

While the standard Hubbard-Stratonovich approach is more appropriate the important terms included in this decoupling is enough to illustrate the phenomena. Here ϕ_{12} is a real valued field. The effective Hamiltonian is

$$\begin{aligned} H_{\text{eff}} &= (t - iV\phi_{12})c_1^\dagger c_2 + (t + iV\phi_{12})c_2^\dagger c_1 + V(n_1 + n_2) \\ &= \frac{t}{\cos(a_{12})} e^{ia_{12}} c_1^\dagger c_2 + \frac{t}{\cos(a_{12})} e^{-ia_{12}} c_2^\dagger c_1 \\ &\quad + V(n_1 + n_2) \end{aligned} \quad (3)$$

where $a_{12} = \arctan\left(-\frac{V\phi_{12}}{t}\right)$. Crucially there is a modification of the hopping matrix element that depends on the value of ϕ_{12} on the link. For a two site model the phase on the link can be eliminated by a gauge transformation and is not physically meaningful. However for any lattice the net flux within a plaquette, i.e. finite sum of phase field a_{ij} , cannot be eliminated. It is important to emphasize that only the phase of the link variable, $e^{ia_{ij}}$ is affected by a gauge transformation, while the modified hopping $t/\cos(a_{ij})$ remains unchanged.

These considerations are analogous to mean field theories where the bond variable is a complex field χ_{12} (rather than just $i\phi_{12}$) whose phase was considered a redundant variable [6, 7]. However the specification of the flux pattern in each unit cell does not uniquely determine the fermionic ground state. Various orderings of χ_{ij} have been considered in the context of Heisenberg Hubbard models on a square lattice leading to a phase diagram that includes the staggered flux phase, Peierls state, and the Kite Phase. The last two are not flux phases but are bond ordered phases involving charge modulation[6].

* yliu545@ucr.edu

† vivek.aji@ucr.edu

II. ONE-BAND MODEL ON A SQUARE LATTICE

A. Model

We consider a one-band model on square lattice which can spontaneously develop a loop current pattern with the same symmetry as the Θ_{II} -loop-current pattern in three-band model[25–28]. The one-band model is effectively captured by the following Hamiltonian of spinless electrons:

$$\begin{aligned} \hat{H} = & -t \sum_{\langle ij \rangle} (\hat{c}_i^\dagger \hat{c}_j + h.c.) - t' \sum_{\langle\langle ij \rangle\rangle} (\hat{c}_i^\dagger \hat{c}_j + h.c.) \\ & + V \sum_{\langle ij \rangle} \hat{n}_i \hat{n}_j, \end{aligned} \quad (4)$$

where t and t' are the nearest-neighbor (NN) and the next-nearest-neighbor (NNN) hopping integrals, respectively. \hat{c}_i labels the annihilation operators of electrons at site \mathbf{R}_i , and \hat{n}_i is the corresponding density operator. For simplicity, we only consider the nearest-neighbor interaction with strength V . The generalization to including interaction along diagonal directions is straightforward but does not change the essential physics for our analysis.

To show how the loop-current phase can spontaneously emerge, we perform mean-field studies of the Hamiltonian in Eq.(4) and rewrite the nearest neighbor interaction by using the identity $2\hat{c}_{i\sigma}^\dagger \hat{c}_{i\sigma} \hat{c}_{j\sigma'}^\dagger \hat{c}_{j\sigma'} = -(\hat{c}_{i\sigma}^\dagger \hat{c}_{j\sigma'} + h.c.)^2 + \hat{n}_{i\sigma} + \hat{n}_{j\sigma'}$. Then up to a constant proportional to the total number of electrons, the nearest neighbor interaction can be rewritten in terms of the bond operator $\hat{J}_{ij} = i(\hat{c}_i^\dagger \hat{c}_j - h.c.)$ as

$$V \sum_{\langle ij \rangle} \hat{n}_i \hat{n}_j \rightarrow -\frac{1}{2} V \sum_{\langle ij \rangle} \hat{J}_{ij}^2. \quad (5)$$

Our primary interest is to establish the most energetically favorable loop current phase. Competition with other orders, e.g. charge density wave order $\langle n_i \rangle$, bond charge density wave $\langle c_i^\dagger c_j + c_j^\dagger c_i \rangle$, or pair density wave $\langle c_i c_j \rangle$, and conditions for when any of the loop current phases identified here are favorable is left for future studies. We decouple the interaction in the ‘‘bond current’’ channel and write the mean-field Hamiltonian as

$$\hat{H}_{\text{MF}} = \hat{H}_0 + \sum_{\langle ij \rangle} \left[\frac{1}{2} V J_{ij}^2 - V J_{ij} \hat{J}_{ij} \right], \quad (6)$$

where H_0 is the free fermion Hamiltonian including the NN and NNN hoppings, and the second term in the bracket amounts to modify the nearest neighbor hopping amplitude as $t \rightarrow t + iVJ_{ij} \equiv Z_{ij}t e^{i\Phi_{ij}}$, and $\Phi_{ij} = \arg[t + iVJ_{ij}] = \tan^{-1}(VJ_{ij}/t)$, $Z_{ij} = 1/\cos \Phi_{ij}$. By substitution of variable $J_{ij} \rightarrow \Phi_{ij}$, we compactify the configuration space of $J_{ij} \in \mathbb{R}$ to $\Phi_{ij} \in (-\pi/2, \pi/2)$. The mean field Hamiltonian in terms of Φ_{ij} fields can be written as

$$\begin{aligned} \hat{H}_{\text{MF}} = & - \sum_{\langle ij \rangle} \frac{t}{\cos \Phi_{ij}} e^{i\Phi_{ij}} \hat{c}_i^\dagger \hat{c}_j - t' \sum_{\langle\langle ij \rangle\rangle} \hat{c}_i^\dagger \hat{c}_j + h.c. \\ & + \sum_{\langle ij \rangle} \frac{1}{2} V J_{ij}^2. \end{aligned} \quad (7)$$

It is worth noting that the resulting modified nearest hopping term is reminiscent of the Peierls substitution for the coupling of fermions to magnetic fluxes. Consequently, the field Φ_{ij} resembles the gauge connection on the links, and we may interpret the gauge invariant quantity $\phi = \sum_{(i,j) \in \Delta(\square)} \Phi_{ij}$ as the flux through the triangle(square) plaquette. Since there are four links and one atom per unit cell, three independent flux configurations are possible. They can be classified as one with spatial s-symmetry which is a net flux through the plaquette and two p-symmetric configurations with net flux zero (see fig.1). A word of caution. These labeling of symmetries is meant to reflect the behavior under spatial rotations.

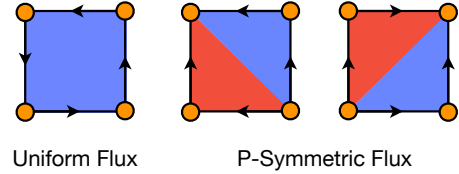


FIG. 1: Possible intra-unitcell flux phases in a square lattice with next nearest neighbor hopping. There is one configuration with a next flux and two with p-symmetry with next zero flux.

We now discuss the possible non-equivalent ansatz that form different flux patterns. To constrain the number of possible ansatz, we only consider the possible translation symmetry broken phases within the $\sqrt{2} \times \sqrt{2}$ unit cell and the order parameter J_{ij} is assumed to be

$$J_{ij} = \sum_{\nu=1}^4 J_\nu \delta_{\mathbf{e}_\nu, \mathbf{e}_{ij}} \quad (8)$$

where $i \in A$ sublattice, $j \in B$ sublattice, $\mathbf{e}_1 = -\mathbf{e}_3 = \mathbf{e}_x$ and $\mathbf{e}_2 = -\mathbf{e}_4 = \mathbf{e}_y$. \mathbf{e}_{ij} is the unit vector connecting site i and j . The mean field Hamiltonian can then be written in terms of 2-component spinor $C_{\mathbf{k}} = (c_{\mathbf{k}A}, c_{\mathbf{k}B})^T$ in the Fourier space,

$$\begin{aligned} \frac{\hat{H}_{\text{MF}}}{N} = & \frac{V}{4} \sum_{\nu=1}^4 J_\nu^2 + \frac{1}{N} \sum_{\mathbf{k}, s=\pm} \hat{C}_{\mathbf{k}}^\dagger h_{\mathbf{k}} \hat{C}_{\mathbf{k}}, \quad (9) \\ h_{\mathbf{k}} = & \begin{pmatrix} -4t' c_x c_y & -\sum_{\nu=1}^4 t_\nu e^{i\mathbf{k} \cdot \mathbf{e}_\nu} \\ -\sum_{\nu=1}^4 t_\nu e^{i\mathbf{k} \cdot \mathbf{e}_\nu} & -4t' c_x c_y \end{pmatrix} \end{aligned} \quad (10)$$

where $c_x \equiv \cos k_x$, $c_y \equiv \cos k_y$. Here $t_\nu = t + iVJ_\nu$ and $\sum_{\mathbf{k}}$ sums over the states in the first Brillouin zone of size $\sqrt{2}\pi \times \sqrt{2}\pi$ as the unit cell is doubled. Diagonalizing \hat{H}_{MF} by a unitary transformation,

$$\begin{pmatrix} \hat{c}_{\mathbf{k}A} \\ \hat{c}_{\mathbf{k}B} \end{pmatrix} = \frac{1}{\sqrt{2}} \begin{pmatrix} e^{i\theta_{\mathbf{k}}/2} & -e^{i\theta_{\mathbf{k}}/2} \\ e^{-i\theta_{\mathbf{k}}/2} & e^{-i\theta_{\mathbf{k}}/2} \end{pmatrix} \begin{pmatrix} \hat{\alpha}_{\mathbf{k}+} \\ \hat{\alpha}_{\mathbf{k}-} \end{pmatrix} \quad (11)$$

with $\theta_{\mathbf{k}} = \arg \left(\sum_{\nu=1}^4 t_\nu e^{i\mathbf{k} \cdot \mathbf{e}_\nu} \right)$, we obtain

$$\frac{\hat{H}_{\text{MF}}}{N} = \frac{V}{4} \sum_{\nu=1}^4 J_\nu^2 + \frac{1}{N} \sum_{\mathbf{k}, s=\pm} \epsilon_{\mathbf{k}s} \hat{\alpha}_{\mathbf{k}s}^\dagger \hat{\alpha}_{\mathbf{k}s}, \quad (12)$$

where s is a band index and the dispersions are given by

$$\epsilon_{\mathbf{k}s} = -4t' \cos k_x \cos k_y + s \left| \sum_{\nu=1}^4 t_\nu e^{i\mathbf{k}\cdot\mathbf{e}_\nu} \right|. \quad (13)$$

For a given temperature and filling factor $\nu = \frac{1}{N} \sum_i c_i^\dagger c_i$, the phase will be favored with the lowest free energy in the canonical ensemble

$$\frac{\mathcal{E}_{\text{MF}}}{N} = \frac{V}{4} \sum_{\mu=1}^4 J_\mu^2 + \frac{1}{N} \sum_{\mathbf{k}, s=\pm} \epsilon_{\mathbf{k}s} n_F(\epsilon_{\mathbf{k}s}), \quad (14)$$

The chemical potential determined through $\frac{1}{2} \sum_{\mathbf{k}s} \Theta(\mu - \epsilon_{\mathbf{k}s}) = N\nu$, where Θ is the step function and the sum is performed over the first Brillouin zone of the underlying square lattice of size $2\pi \times 2\pi$.

B. Mean field phase diagram

We performed numerical calculations on a square lattice of size $N = 100 \times 100$ at zero temperature. Notice that the total energy is symmetric under $G = \{D_4, D_4T\}$ operations of (J_1, J_2, J_3, J_4) , i.e. $\mathcal{E}_{\text{MF}}[J_1, J_2, J_3, J_4] = \mathcal{E}_{\text{MF}}[(J_1, J_2, J_3, J_4)^g]$ ($g \in G$), where D_4 is the dihedral group of a square, T is the time-reversal operation that flips the sign of all J 's, and $(J_1, J_2, J_3, J_4)^g$ is the action of a group element g on the tuple (J_1, J_2, J_3, J_4) . To reduce the search space, we impose symmetry breaking constraints that retain only one representative (flux pattern) in each symmetry class. This approach leverages lexicographic ordering constraints (LOC) [29, 30] as a method for symmetry reduction.

1. Lexicographic order

For two vectors x, y in \mathbb{R}^n the lexicographic order is defined inductively as

$$\begin{aligned} (x_1, \dots, x_n) \preceq_{lex} (y_1, \dots, y_n) &\equiv (x_1 < y_1) \vee \\ &((x_1 = y_1) \wedge (x_2, \dots, x_n) \preceq_{lex} (y_2, \dots, y_n)). \end{aligned} \quad (15)$$

Given a symmetry $g \in G$ of the parameter space, we define the corresponding symmetry-breaking constraint as $\text{LEX}_g(x) = x \preceq_{lex} x^g$. For example, let r be a rotation by $\pi/2$, then $\text{LEX}_r(J_1, J_2, J_3, J_4) = (J_1, J_2, J_3, J_4) \preceq_{lex} (J_4, J_1, J_2, J_3)$. The complete symmetry-breaking constraint then is the conjunction of all $\text{LEX}_g(x)$, i.e. $\text{LEX}_G(x) = \bigwedge_{g \in G} \text{LEX}_g(x)$. For instance, with D_4 symmetry,

$$\begin{aligned} \text{LEX}_{D_4}(J_1, J_2, J_3, J_4) &= (J_1 = J_2 \leq J_3 \leq J_4) \vee \\ &(J_1 \leq J_3 < J_2 \leq J_4) \vee (J_1 < J_2 \leq J_3 \wedge J_2 \leq J_4). \end{aligned} \quad (16)$$

The reduced search space then is $S_G = \{x \in \mathbb{R}^n | \text{LEX}_G(x)\}$. For finite groups with large order, managing multiple complex orders makes them impractical for numerical constraint satisfaction problems. However, this complexity associated the boundaries of the reduced search space can be simplified, given that the boundaries are normally negligible in numerical domains. To do this, we follow Ref.[30] and consider the relaxed LEX constraint defined as $\text{RLEX}_g(x) \equiv (x)_{n_g} \leq (x^g)_{n_g}$. Here $(x)_{n_g}$ is the n_g -th component of x and is the smallest number that satisfies $(x)_{n_g} \neq (x^g)_{n_g}$. For a rotation by $\pi/2$, $\text{RLEX}_r(J_1, J_2, J_3, J_4) = J_1 \leq J_4$; and for a rotation by π around x -axis σ_x , $\text{RLEX}_{\sigma_x}(J_1, J_2, J_3, J_4) = J_4 \leq J_2$. It turns out that the corresponding search space generated by RLEX order is the closure of that generated by LEX order [30]. Therefore, we have the following relaxed constraints:

$$\text{RLEX}_G(J_1, J_2, J_3, J_4) = (J_1 \leq J_2 \leq J_4) \wedge (J_1 \leq J_3) \wedge (J_1 \leq 0) \wedge (J_2 \leq -J_1) \wedge (J_3 \leq -J_1) \wedge (J_4 \leq -J_1). \quad (17)$$

2. Phase diagram

In Fig. 2, the zero-temperature mean field phase diagram is presented, obtained by minimizing the total energy with respect to the parameters (J_1, J_2, J_3, J_4) across various doping levels and interaction strengths. This optimization utilizes the Simplicial Homology Global Optimization (SHGO) algorithm [31], combined with the constraints in 17. We set $t = 1$ eV, $t' = 0.2$ eV and the cutoff strength of V to be around 5 eV, above which V exceeds the the band-width. We examine two scenarios: one with a finite net flux within the square plaquette, and the other without.

Phase diagram 1: Our result shows a rich phase diagram over wide range of the (V, ν) plane. The phases can be divided to three classes. (1) Fermi liquid states without flux which include phases A and N: Phase A has all J_{MF} 's being the same on the links but it still corresponds to zero flux state. This is because the relative phase that appears

in the effective hoppings $t + iJ_{\text{MF}} = t/\cos(\Phi)e^{i\Phi}$ can be removed by a gauge transformation $c_{iA(B)} \rightarrow e^{i\theta_{A(B)}} c_{iA(B)}$ with $\theta_B - \theta_A = \Phi$. Moreover, phase A does not break any lattice symmetry as the magnitude of J_{MF} (and thus the effect hopping) is the same everywhere. (2) Θ_{II} (see [12]) like phases which include phases B, G and D: These three phases have the same symmetries as the Θ_{II} loop current order in the flux sector. The presence of flux within triangle plaquettes explicitly breaks time reversal symmetry and C_4 symmetry, while the lattice translational symmetry is respected by the flux. Although phases B and G have translational symmetry in the flux sector, they break the translational symmetry in the distribution of J_{ij} on the links. This has consequences for the electronic sector and the symmetry of of the lattice. Phase D corresponds to the canonical Θ_{II} (see [12]) preserving lattice translational symmetry in all sectors. (3) Staggered flux phases that include phases E, F and G: Phase E has the same magnitude of J_{ij} on the links, and it explicitly breaks time reversal

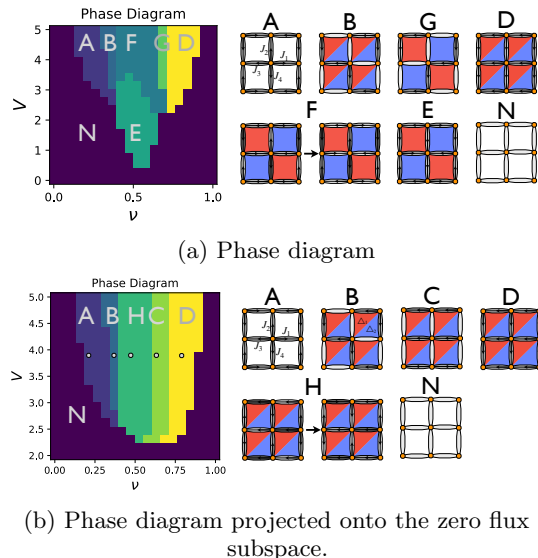


FIG. 2: Mean-field phase diagram in the (ν, V) plane at fixed $t = 1$ eV, $t' = 0.2$ eV. The arrow denotes the direction of J_{ij} , and the gray scale represents the magnitude of J_{ij} .

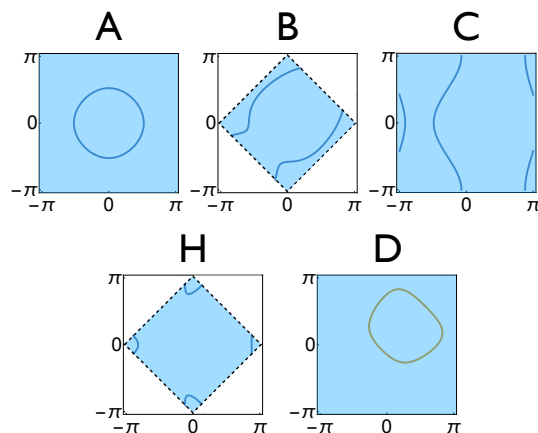


FIG. 3: Typical Fermi surfaces at gray dots in the zero-flux phase diagram. The shaded area denotes the Brillouin zone.

symmetry and also breaks C_4 down to C_2 . Phase F is a collection of phases with one J in (J_1, J_2, J_3, J_4) being the largest. Phase G is characterized by two non-vanishing J_{ij} 's on the links in the enlarged unit cell which resembles the

stripe phase.

Phase diagram 2: We now focus on the subspace of flux phases with vanishing net flux per unit cell. This represents the cases where additional terms in the Hamiltonian are present, such as $H' \sim U(\sum_{(i,j) \in \square} \Phi_{ij})^2$, which restrict the low energy sector to the p-symmetric states. Our numerical result shows that the previous staggered flux phases now are replaced by phase C and H near the half filling $\nu = 0.5$. Phase C respects lattice translational symmetry for the flux but has stripe-like bond order J_{MF} . Phase H represents a collection of phases where one bond order J in (J_1, J_2, J_3, J_4) is the largest.

3. Fermi surfaces

In this section, we discuss the evolution of Fermi surfaces within the zero-flux phase diagram at a fixed interaction strength ($V \approx 4$ eV) as the filling factor is varied. Our results are shown in Fig. 3 for the ground state in a single domain. Phase A does not break any symmetry but has renormalized hopping. Hence the symmetry of the Fermi surface is unchanged. Phases B and C both break translational and rotational symmetries. They have stripe-like ordering resulting in open Fermi surfaces. Phase H leads to electron pockets at $(\pi, 0)$ and $(0, \pi)$. Phase D is translationally invariant but has broken rotational symmetry. These results underscore the central point of this paper which is that the symmetry of the flux sector within unit cells do not uniquely determine the ground state of the system.

C. Discussion and Summary

In this work, we have studied a spinless-fermion model on a square lattice, in which the nearest-neighbor interaction can be written in terms of bond-current operators, giving rise to various flux phases that breaks time-reversal. Contrary to previous studies on flux phases, we have shown in this simple model that flux pattern cannot uniquely determine the fermionic ground state. This main conclusion calls for further studies of the validity of the arbitrary assignments of gauge fields on the links for flux phases driven by interaction. An open question to be studied in the future is the competitiveness of this class of states with other forms of symmetry breaking in the charge and spin sector. Future studies will report on lattice models which include nearest neighbor repulsion using methods that better capture fluctuations beyond mean field.

[1] F. D. M. Haldane, Model for a quantum hall effect without landau levels: Condensed-matter realization of the "parity anomaly", *Phys. Rev. Lett.* **61**, 2015 (1988).
 [2] C. L. Kane and E. J. Mele, Quantum spin hall effect in graphene, *Phys. Rev. Lett.* **95**, 226801 (2005).
 [3] K. Sun and E. Fradkin, Time-reversal symmetry breaking and spontaneous anomalous hall effect in fermi fluids, *Phys. Rev. B* **78**, 245122 (2008).
 [4] E. V. Castro, A. G. Grushin, B. Valenzuela, M. A. H. Vozmediano, A. Cortijo, and F. de Juan, Topological fermi liquids from coulomb interactions in the doped honeycomb

lattice, *Phys. Rev. Lett.* **107**, 106402 (2011).
 [5] S. Sur, S.-S. Gong, K. Yang, and O. Vafek, Quantum anomalous hall insulator stabilized by competing interactions, *Phys. Rev. B* **98**, 125144 (2018).
 [6] I. Affleck and J. B. Marston, Large- n limit of the heisenberg-hubbard model: Implications for high- T_c superconductors, *Phys. Rev. B* **37**, 3774 (1988).
 [7] J. B. Marston and I. Affleck, Large- n limit of the hubbard-heisenberg model, *Phys. Rev. B* **39**, 11538 (1989).
 [8] M. U. Ubbens and P. A. Lee, Flux phases in the $t - J$ model, *Phys. Rev. B* **46**, 8434 (1992).

- [9] S. Chakravarty, R. B. Laughlin, D. K. Morr, and C. Nayak, Hidden order in the cuprates, *Phys. Rev. B* **63**, 094503 (2001).
- [10] M. Yamanaka, W. Koshibae, and S. Maekawa, “flux” state in the double-exchange model, *Phys. Rev. Lett.* **81**, 5604 (1998).
- [11] C. M. Varma, Non-fermi-liquid states and pairing instability of a general model of copper oxide metals, *Phys. Rev. B* **55**, 14554 (1997).
- [12] C. M. Varma, Theory of the pseudogap state of the cuprates, *Physical Review B (Condensed Matter and Materials Physics)* **73**, 155113 (2006).
- [13] C. M. Varma, Considerations on the mechanisms and transition temperatures of superconductivity induced by electronic fluctuations, *Reports on Progress in Physics* **75**, 052501 (2012).
- [14] B. Fauqué, Y. Sidis, V. Hinkov, S. Pailhès, C. T. Lin, X. Chaud, and P. Bourges, Magnetic order in the pseudogap phase of high- T_c superconductors, *Physical Review Letters* **96**, 197001 (2006).
- [15] H. A. Mook, Y. Sidis, B. Fauqué, V. Balédent, and P. Bourges, Observation of magnetic order in a superconducting $YBa_2Cu_3O_{6.6}$ single crystal using polarized neutron scattering, *Physical Review B (Condensed Matter and Materials Physics)* **78**, 020506 (2008).
- [16] V. Scagnoli, U. Staub, Y. Bodenthin, R. A. de Souza, M. Garc a-Fern andez, M. Garganourakis, A. T. Boothroyd, D. Prabhakaran, and S. W. Lovesey, Observation of orbital currents in CuO , *Science* **332**, 696 (2011), <http://www.sciencemag.org/content/332/6030/696.full.pdf>.
- [17] J. , E. Schemm, G. Deutscher, S. A. Kivelson, D. A. Bonn, W. N. Hardy, R. Liang, W. Siemons, G. Koster, M. M. Fejer, and A. Kapitulnik, Polar kerr-effect measurements of the high-temperature $YBa_2Cu_3O_{6+x}$ superconductor: Evidence for broken symmetry near the pseudogap temperature, *Phys. Rev. Lett.* **100**, 127002 (2008).
- [18] A. R ugg and G. A. Fiete, Topological insulators from complex orbital order in transition-metal oxides heterostructures, *Phys. Rev. B* **84**, 201103 (2011).
- [19] K.-Y. Yang, W. Zhu, D. Xiao, S. Okamoto, Z. Wang, and Y. Ran, Possible interaction-driven topological phases in (111) bilayers of $lanio_3$, *Phys. Rev. B* **84**, 201104 (2011).
- [20] S. Raghu, X.-L. Qi, C. Honerkamp, and S.-C. Zhang, Topological mott insulators, *Phys. Rev. Lett.* **100**, 156401 (2008).
- [21] J. Motruk, A. G. Grushin, F. de Juan, and F. Pollmann, Interaction-driven phases in the half-filled honeycomb lattice: An infinite density matrix renormalization group study, *Phys. Rev. B* **92**, 085147 (2015).
- [22] C. N. Varney, K. Sun, M. Rigol, and V. Galitski, Interaction effects and quantum phase transitions in topological insulators, *Phys. Rev. B* **82**, 115125 (2010).
- [23] Y. Zhang, Y. Ni, H. Zhao, S. Hakani, F. Ye, L. DeLong, I. Kimchi, and G. Cao, Control of chiral orbital currents in a colossal magnetoresistance material, *Nature* **611**, 467 (2022).
- [24] C. Mielke, D. Das, J. X. Yin, H. Liu, R. Gupta, Y. X. Jiang, M. Medarde, X. Wu, H. C. Lei, J. Chang, P. Dai, Q. Si, H. Miao, R. Thomale, T. Neupert, Y. Shi, R. Khasanov, M. Z. Hasan, H. Luetkens, and Z. Guguchia, Time-reversal symmetry-breaking charge order in a kagome superconductor, *Nature* **602**, 245 (2022).
- [25] A. Allais and T. Senthil, Loop current order and d-wave superconductivity: Some observable consequences, *Physical Review B* **86**, 045118 (2012).
- [26] S. Kivelson and C. Varma, Fermi pockets in a d-wave superconductor with coexisting loop-current order, *arXiv preprint arXiv:1208.6498* (2012).
- [27] T. D. Stanescu and P. Phillips, Nonperturbative approach to full mott behavior, *Physical Review B* **69**, 245104 (2004).
- [28] L. Wang and O. Vafek, Quantum oscillations of the specific heat in d-wave superconductors with loop current order, *Physical Review B* **88**, 024506 (2013).
- [29] I. P. Gent, K. E. Petrie, and J.-F. Puget, Symmetry in constraint programming, *Foundations of Artificial Intelligence* **2**, 329 (2006).
- [30] A. Goldsztejn, C. Jermann, V. R. de Angulo, and C. Torras, Variable symmetry breaking in numerical constraint problems, *Artificial Intelligence* **229**, 105 (2015).
- [31] S. C. Endres, C. Sandrock, and W. W. Focke, A simplicial homology algorithm for lipschitz optimisation, *Journal of Global Optimization* **72**, 181 (2018).